Journal of Modern Optics
Vol. 00, No. 00, 00 Month 200x, 1–13

Special issue on "Single Photon Technologies"

Engineering of optical continuous-variable qubits via displaced photon subtraction: Multimode analysis

M. Takeoka, J. S. Neergaard-Nielsen, M. Takeuchi, K. Wakui, H. Takahashi, K. Hayasaka, and M. Sasaki
National Institute of Information and Communications Technology
4-2-1 Nukui-kitamachi, Koganei, Tokyo 184-8795, Japan
(*Received 00 Month 200x; final version received 00 Month 200x*)

We investigate the practical scheme of engineering a qubit of two optical continuous-variable states, based on squeezed vacuum and coherently displaced photon subtraction. A fully multimode model is developed to describe a cw setting of the experiment, which has been successfully implemented to generate highly pure nonclassical states. The model agrees well with the experimental results and the numerical results show that the intrinsic imperfection due to the cw nature of the source is relatively small. Our photon subtraction technique could also be useful for preparing optical Schrödinger's cat-like states in arbitrary superposition, which is a basic qubit resource for linear optics coherent state quantum computing.

Keywords: photon subtraction; squeezed state; continuous-variable qubit; coherent state quantum computing

1. Introduction

Single-photon or photon-number-resolving detection is an important technology in photonic-qubit based quantum information processing (QIP) as well as continuous-variable (CV) QIP. One can subtract photons from a traveling wave without disturbing it by sending it through a highly transmissive beam splitter and detecting photons in the reflected beam. Selecting the event such that n photons are detected, one obtains a conditional output state in which n photons are subtracted, in other words, annihilation operations $\hat{a}^n$ are applied. Photon subtraction is a powerful and practical technique in optical QIP and has been successfully used for nonclassical state generation (*1–7*), entanglement increase (*8, 9*), and fundamental tests of quantum mechanics (*10*). In particular, attention has been paid to the generation of optical Schrödinger cat-like states, i.e. quantum superposition of classical states (coherent states), via photon subtraction. Optical cat-like states are important not only for testing fundamental quantum mechanics, but also as useful resources of linear optical coherent state quantum computing (CSQC) (*11–15*). The scheme uses two phase-opposite coherent states $|\pm\alpha\rangle$ as (quasi-)qubit bases and consists of off-line resource states, linear optics, and photon number resolving detectors.

In addition to exponential speed-up of computation, CSQC is effective for approaching the ultimate capacity of optical communications. The basic channel coding theorem extending Shannon's conventional theory into the quantum domain has been developed (*16*) and recently the channel capacity of lossy optical channels was derived (*17*). These results showed that the capacity in a lossy optical channel is attainable with simple coherent state-encoding but the optimal decoding should be a large-scale nontrivial collective quantum measurement. The importance of collective decoding in a finite-length coding scenario has been discussed (*18*) and the proof-of-principle of collective decoding based on a quantum computing circuit has been demonstrated with single-photon qubits (*19, 20*). However, it is still a big challenge to implement a practical CSQC even for a small scale circuit − one requirement is the availability of arbitrary qubit states

ISSN: 0950-0340 print/ISSN 1362-3044 online

DOI: 10.1080/0950034YYxxxxxxxx
http://www.informaworld.com

in coherent state basis. So far, only two diagonal cat-like states of the qubit $|\alpha\rangle \pm |-\alpha\rangle$ have been generated in the laboratories (*1–6*).

Recently, we have proposed a scheme of generating such arbitrary qubits (*21*) and demonstrated its basic operation in the laboratory (*22*). For the demonstration, we performed the complete engineering of a different, but closely related kind of qubit, namely one with squeezed vacuum and squeezed single-photon states as the basis. The squeezed photon state is in fact very similar to one of the CSQC diagonal qubits, as was utilized in the previous demonstrations of those. In the experiment, a cw source was used for preparing squeezed states. The cw source of squeezed state is intuitively regarded as a continuous sequence of squeezed wave packets. The photon subtraction conditionally makes a squeezed qubit state in one of these packets and one has to be careful how to extract that wave packet at the state detection step.

In this paper, we theoretically elaborate a multimode model describing an arbitrary squeezed qubit generation from a cw squeezed state. The paper contains the following new aspects. First, we describe a full multimode model in detail which takes into account practical parameters and show that our model agrees well with the experiment demonstrated in (*22*). Second, we numerically investigate the fundamental discrepancy between the cw model and the single mode model. Due to the multimode character of a cw source, even for an ideal, lossless model, the cw scheme cannot create an ideal squeezed qubit. We clarify quantitative state dependent degradations of the fidelity and show that this fundamental limitation does not seriously destroy the states in practice. Finally, we represent the density matrices of squeezed qubit states in the cw scheme in terms of a squeezed photon number basis and compare these with the standard photon number state basis density matrices. The result clearly shows that while our qubits are CV states these also exist in a superposition of two well-defined orthogonal states. The paper is organized as follows. In Sec. 2, we briefly review the simplified single-mode scheme for the squeezed qubit generation and its fully multimode model is described in detail in Sec. 3. The numerical analyses including the comparison to the experimental results are shown in Sec. 4. Section 5 concludes the paper.

2. Photon subtraction assisted by coherent displacement

We start by reviewing a simplified single-mode model to illustrate the intuitive understanding of our photon subtraction scheme (*21, 22*). The schematic is shown in Fig. 1(a). A single-mode squeezed vacuum state $\hat{S}_A(r)\,|0_A\rangle$ is prepared in mode A, where $\hat{S}_A(r) = \exp\{\frac{r}{2}(\hat{a}^{\dagger\,2} - \hat{a}^2)\}$ represents the squeezing operation with strength r. A small fraction R of it is tapped off via a beam splitter, $\hat{V}_{AB} = \exp\{\sigma(\hat{a}^\dagger\hat{b} - \hat{a}\hat{b}^\dagger)\}$ with $R = \sin^2\sigma$, as a trigger beam in mode B. The trigger beam is then subjected to the displacement operation $\hat{D}_B(\beta) = \exp(\beta\hat{b}^\dagger - \beta^*\hat{b})$, and detected on an avalanche photodiode (APD). It is well known that a displacement operation is realized by a highly transmissive beam splitter and a local oscillator.

Let us assume that R and $|\beta|^2$ are sufficiently small such that the APD detects at most one photon and $\ln(1-R) \approx 0$. The unnormalized output state conditioned on an APD click is then given by

$$\begin{aligned} |\tilde{\Psi}\rangle &\approx \langle 1_B|\,\hat{D}_B(\beta)\hat{V}_{AB}\hat{S}_A(r)\,|0_{AB}\rangle \\ &\approx \langle 0_B|\,\hat{D}_B(\beta)(\beta + \sqrt{R}\hat{a}_A)\hat{S}_A(r)\,|0_{AB}\rangle \\ &\approx \beta\hat{S}_A(r)\,|0_A\rangle - \sqrt{R}\sinh r\hat{S}_A(r)\,|1_A\rangle\,, \end{aligned} \tag{1}$$

with success probability

$$P_{\rm on} \approx |\beta|^2 + R\sinh^2 r = n_{\rm disp} + n_{\rm sq}, \tag{2}$$

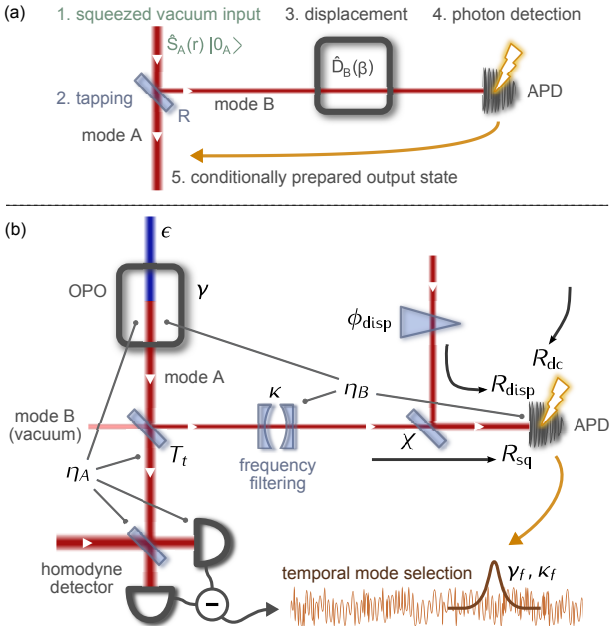

Figure 1. Experimental outline. (a) Simplified single-mode model. (b) Experimental setup with symbols defined in the text. OPO, optical parametric oscillator; R, beam splitter reflectivity; LO, local oscillator; APD, avalanche photo diode. See Table 1 for the other parameters.

where $n_{\rm disp}$ ($n_{\rm sq}$) are the number of photons in mode B originating from the displacement beam (squeezing).

Equation (1) shows that the conditional output state is a coherent superposition of a squeezed vacuum $\hat{S}(r)\,|0\rangle$ and a 1-photon subtracted squeezed vacuum which is equivalent to a squeezed photon $\hat{S}(r)\,|1\rangle$. Such a superposition originates from the two indistinguishable events, i.e. an APD click coming either from the displacement or from the squeezing, and its weight and phase can be controlled by the parameters of the displacement operation. Each of the two states is composed of several Fock state elements – only even photon numbers for $\hat{S}(r)\,|0\rangle$ and odd numbers for $\hat{S}(r)\,|1\rangle$. They are orthogonal to each other, so together they constitute a qubit basis. Therefore, after the normalization, the general output state (1) can be represented on a Bloch sphere as

$$\begin{aligned} |{\rm SQ}(\theta,\varphi)\rangle &= \frac{1}{\sqrt{P_{\rm on}}}\left(\beta\hat{S}(r)\,|0\rangle - \sqrt{R}\sinh r\hat{S}(r)\,|1\rangle\right), \\ &= \cos\frac{\theta}{2}\hat{S}(r)\,|0\rangle + e^{i\varphi}\sin\frac{\theta}{2}\hat{S}(r)\,|1\rangle\,, \end{aligned} \tag{3}$$

with $\varphi = \pi - \arg\beta$ and

$$\cos\frac{\theta}{2} = \frac{|\beta|}{\sqrt{|\beta|^2 + R\sinh^2 r}} = \sqrt{\frac{n_{\rm disp}}{n_{\rm disp}+n_{\rm sq}}}. \tag{4}$$

3. Multimode model

3.1. *Experimental setting*

In this section, we connect the scheme given in the last section and the experiment performed in (*22*) by describing a precise theoretical modeling which fully takes into account temporal

γ	OPO bandwidth	$2\pi\times$4.5 MHz
ϵ	pump level	variable – in the experiment (*22*), 0.3γ
κ	filter bandwidth	$\sim 2\pi\times$25 MHz
T_t	tapping BS transmission	0.95
η_A	overall efficiency, signal	0.82 ($0.96\times 0.91\times 0.98^2\times 0.99\times 0.99$)
η_B	overall efficiency, trigger	~ 0.1
$R_{\rm sq}$	click rate, squeezed photons	variable – in the experiment (*22*), 3600 c/s
$R_{\rm disp}$	click rate, displacement photons	variable – typically 50-50,000 c/s
$R_{\rm dc}$	click rate, dark counts	$\sim$30 c/s
$\phi_{\rm disp}$	displacement angle	variable
χ	displacement mode matching	0.97

Table 1. Model parameters and typical experimental values. The factors of the signal efficiency are: OPO escape, propagation, LO visibility, quantum efficiency, dark noise.

multimodes of the cw sources and relevant experimental parameters. The experimental setup is illustrated in Fig. 1(b). Initially, a cw squeezed vacuum is generated by a sub-threshold optical parametric oscillator (OPO) into mode A. The OPO HWHM bandwidth is γ and the pump level is $\epsilon<\gamma$. We align the phase space to have squeezing in the p-quadrature. The normal ordered temporal output correlations are then (*23*)

$$\langle{:}\Delta\hat{x}_{\rm A,ini}(t)\Delta\hat{x}_{\rm A,ini}(t'){:}\rangle=\frac{\gamma\epsilon}{\gamma-\epsilon}e^{-(\gamma-\epsilon)|t-t'|}, \tag{5}$$

$$\langle{:}\Delta\hat{p}_{\rm A,ini}(t)\Delta\hat{p}_{\rm A,ini}(t'){:}\rangle=-\frac{\gamma\epsilon}{\gamma+\epsilon}e^{-(\gamma+\epsilon)|t-t'|}. \tag{6}$$

The squeezed vacuum is split on a beam splitter with transmission T_t, being mixed with vacuum from mode B. The transmitted beam is the output signal to be recorded by the homodyne detector whose overall efficiency we denote by η_A – this efficiency parameter includes homodyne visibility, propagation losses, etc., as well as the effect of internal losses in the OPO which are easy to measure independently. The reflection is sent towards an APD, being displaced on the way (after frequency filtering) by mixing it with a coherent beam. The details of the displacement process are not important: What matters is the rate of APD clicks originating from the squeezed light, $R_{\rm sq}$, or from the displacement beam, $R_{\rm disp}$ – a click coming from the squeezed light heralds a photon subtraction in mode A, while a click coming from the displacement beam (uncorrelated with mode A) heralds no action.

Other important parameters are the spatial mode matching between trigger and displacement beam, χ, the dark count rate, $R_{\rm dc}$, the overall efficiency of mode B (trigger), η_B, the trigger filter bandwidth (*24*), κ, and the phase angle of displacement, $\phi_{\rm disp}$. The spatial mode matching χ must be close to 1. If not, the two possible origins of the detected photon are not indistinguishable, leading to a mixed state instead of a superposition.

The parameters used in this model together with their typical experimental values are listed in Table 1. Apart from these, there are also the parameters that define the signal mode function as used in the extraction of the homodyne data: γ_f and κ_f. These can be chosen freely, but we usually use the experimentally-equivalent values, that is, $\gamma_f=\gamma$, $\kappa_f=\kappa$.

3.2. *General output state formalism*

To describe the effect of the photon subtraction, we adopt the Wigner formalism of Ref. (*25*). The two-mode state prior to the photon detection event is Gaussian, i.e. it has a Gaussian Wigner function fully determined by the covariance matrix Γ and displacement vector $\mathbf{d}$:

$$W_G(x_A,p_A,x_B,p_B)=\frac{1}{\pi^2\sqrt{\det\Gamma}}e^{-(\mathbf{x}-\mathbf{d})^T\Gamma^{-1}(\mathbf{x}-\mathbf{d})}, \tag{7}$$

with $\mathbf{x} = (x_A, p_A, x_B, p_B)^T$.

To get the state conditional on an APD click in mode B, the Gaussian Wigner function should be multiplied by the Wigner function corresponding to the detection operation and integrated over mode B – this corresponds to $\mathrm{tr}_B[\hat{\rho}_{AB}\hat{\Pi}_B]$ in the density matrix formulation. For the non-photon number resolving APD, we use the standard on/off operation $\hat{\Pi}_{\mathrm{on}} = \hat{I} - |0\rangle\langle 0|$, which has the equivalent Wigner function

$$W_{\mathrm{on}}(x,p) = W_{\mathrm{id}}(x,p) - W_{\mathrm{vac}}(x,p) = \frac{1}{2\pi} - \frac{1}{\pi}e^{-x^2-p^2}. \tag{8}$$

The output state conditioned on a displaced 1-photon subtraction is therefore

$$W_{\mathrm{d-1ps}}(x_A,p_A) = \mathcal{N}_{\mathrm{out}}\, 2\pi \iint_{-\infty}^{\infty} W_G(x_A,p_A,x_B,p_B) W_{\mathrm{on}}(x_B,p_B)\, dx_B dp_B, \tag{9}$$

with normalization to be determined by integrating the output state.

3.2.1. Including dark counts and mode matching

If an APD click is a dark count or if it comes from the part of the displacement beam that is not mode-matched to the trigger beam, there is no action on the signal beam and the output state is simply a squeezed vacuum state

$$W_{\mathrm{sq}}(x_A,p_A) = 2\pi \iint_{-\infty}^{\infty} W_G(x_A,p_A,x_B,p_B) W_{\mathrm{id}}(x_B,p_B)\, dx_B dp_B \tag{10}$$

$$= \iint_{-\infty}^{\infty} W_G(x_A,p_A,x_B,p_B)\, dx_B dp_B. \tag{11}$$

If, on the other hand, the click originates from the trigger beam, but from the part which is not mode-matched to the displacement beam, the result will be a normal un-displaced photon subtraction:

$$W_{\mathrm{1ps}}(x_A,p_A) = \mathcal{N}_{\mathrm{out}}\, 2\pi \iint_{-\infty}^{\infty} W_{\mathrm{G,nd}}(x_A,p_A,x_B,p_B) W_{\mathrm{on}}(x_B,p_B)\, dx_B dp_B. \tag{12}$$

with the un-displaced Gaussian state

$$W_{\mathrm{G,nd}}(x_A,p_A,x_B,p_B) = \frac{1}{\pi^2\sqrt{\det\Gamma}} e^{-\mathbf{x}^T\Gamma^{-1}\mathbf{x}}\ . \tag{13}$$

Let the total count rate be $R = R_{\mathrm{sq}} + R_{\mathrm{disp}} + R_{\mathrm{dc}}$. The final output state is then (with (x_A, p_A) temporarily removed)

$$\begin{aligned} W_{\mathrm{out}} &= \frac{R_{\mathrm{sq}}+R_{\mathrm{disp}}}{R}\left(\chi W_{\mathrm{d-1ps}} + (1-\chi)\left(\frac{R_{\mathrm{disp}}}{R_{\mathrm{sq}}+R_{\mathrm{disp}}}W_{\mathrm{sq}}\ + \frac{R_{\mathrm{sq}}}{R_{\mathrm{sq}}+R_{\mathrm{disp}}}W_{\mathrm{1ps}}\right)\right) + \frac{R_{\mathrm{dc}}}{R}W_{\mathrm{sq}} \\ &= \chi\frac{R_{\mathrm{sq}}+R_{\mathrm{disp}}}{R}W_{\mathrm{d-1ps}} + (1-\chi)\frac{R_{\mathrm{sq}}}{R}W_{\mathrm{1ps}} + \left((1-\chi)\frac{R_{\mathrm{disp}}}{R} + \frac{R_{\mathrm{dc}}}{R}\right)W_{\mathrm{sq}}\ . \end{aligned} \tag{14}$$

3.2.2. Explicit Wigner function

Any two-mode Gaussian state can – via local operations – be put on the following generic form:

$$\Gamma = \begin{pmatrix} a & 0 & e & 0 \\ 0 & b & 0 & f \\ e & 0 & c & 0 \\ 0 & f & 0 & d \end{pmatrix}, \quad \mathbf{d} = \begin{pmatrix} r \\ s \\ t \\ u \end{pmatrix}. \tag{15}$$

By having aligned the squeezing quadrature of the initial state along one of the phase space axes, we have already obtained this form (see next subsection), where the x and p variables are completely decoupled. We can set $r = s = 0$ as displacement only occurs in mode B.

When inserting Γ and $\mathbf{d}$ in (7) and carrying out the integrations, we get the following normalized expressions for the three state components of (14):

$$W_{\rm sq}(x_A, p_A) = \frac{1}{\pi\sqrt{ab}} e^{-\frac{1}{a}x_A^2 - \frac{1}{b}p_A^2}, \tag{16}$$

$$W_{\rm 1ps}(x_A, p_A) = \frac{1}{1-w}\frac{1}{\pi\sqrt{ab}} e^{-\frac{1}{a}x_A^2 - \frac{1}{b}p_A^2} - \frac{w}{1-w}\frac{1}{\pi\sqrt{a'b'}} e^{-\frac{1}{a'}x_A^2 - \frac{1}{b'}p_A^2}, \tag{17}$$

$$W_{\rm d-1ps}(x_A, p_A) = \frac{1}{1-w_d}\frac{1}{\pi\sqrt{ab}} e^{-\frac{1}{a}x_A^2 - \frac{1}{b}p_A^2} - \frac{w_d}{1-w_d}\frac{1}{\pi\sqrt{a'b'}} e^{-\frac{1}{a'}(x_A-r_d)^2 - \frac{1}{b'}(p_A-s_d)^2}, \tag{18}$$

with

$$a' = a - \frac{e^2}{1+c}, \quad b' = b - \frac{f^2}{1+d}, \tag{19}$$

$$r_d = -\frac{et}{1+c}, \quad s_d = -\frac{fu}{1+d}, \tag{20}$$

$$w = \frac{2}{\sqrt{(1+c)(1+d)}}, \qquad w_d = \frac{2}{\sqrt{(1+c)(1+d)}} e^{-t^2/(1+c) - u^2/(1+d)}. \tag{21}$$

The photon subtracted states are just the difference between two squeezed states. For the total state, we can then gather terms to get

$$\begin{aligned} W_{\rm out}(x_A, p_A) = &\left(\chi \frac{R_{\rm sq} + R_{\rm disp}}{R} \frac{1}{1-w_d} + (1-\chi)\frac{R_{\rm sq}}{R}\frac{1}{1-w} + \frac{(1-\chi)R_{\rm disp} + R_{\rm dc}}{R} \right) \\ &\times \frac{1}{\pi\sqrt{ab}} e^{-\frac{1}{a}x_A^2 - \frac{1}{b}p_A^2} \quad - \quad (1-\chi)\frac{R_{\rm sq}}{R}\frac{w}{1-w}\frac{1}{\pi\sqrt{a'b'}} e^{-\frac{1}{a'}x_A^2 - \frac{1}{b'}p_A^2} \\ &- \chi \frac{R_{\rm sq} + R_{\rm disp}}{R}\frac{w_d}{1-w_d}\frac{1}{\pi\sqrt{a'b'}} e^{-\frac{1}{a'}(x_A-r_d)^2 - \frac{1}{b'}(p_A-s_d)^2}. \end{aligned} \tag{22}$$

3.3. *Physical description of state before trigger detection*

The remaining task is to relate the generalized variables of the covariance matrix and displacement vector in Eq. (15) to experimental parameters. The two-mode Gaussian state before the trigger detection has temporal correlations given by the OPO output correlations (5)-(6), by the trigger filtering and by losses. The APD click automatically defines a temporally localized single mode of the trigger beam, and based on the click time, we define a localized mode for the

signal beam. Although this mode selection occurs after the actual photon subtraction, it is possible in the model to impose it on the initial Gaussian state, in order to get a time-independent covariance matrix and displacement vector.

3.3.1. Covariance matrix

The initial time-dependent covariance matrix is modified by the tapping beam splitter, losses, and the mode selection. The handling of covariance matrix transformations is simplified a little by using normal ordering - we do not have to account for the vacuum contributions until the end.

The initial two-mode time-dependent covariance matrix is

$$:\Gamma_{\rm OPO}(t-t'):=\begin{pmatrix} :\Gamma_{\rm OPO,11}: & 0 & 0\ 0 \\ 0 & :\Gamma_{\rm OPO,22}: & 0\ 0 \\ 0 & 0 & 0\ 0 \\ 0 & 0 & 0\ 0 \end{pmatrix}, \tag{23}$$

with

$$:\Gamma_{\rm OPO,11}: = 2\langle :\Delta\hat{x}_{\rm A,ini}(t)\Delta\hat{x}_{\rm A,ini}(t'):\rangle, \tag{24}$$

$$:\Gamma_{\rm OPO,22}: = 2\langle :\Delta\hat{p}_{\rm A,ini}(t)\Delta\hat{p}_{\rm A,ini}(t'):\rangle. \tag{25}$$

The tapping beam splitter, represented by the matrix $V(T_t)$, transforms it to

$$:\Gamma_{\rm bs}(t-t'):= V(T_t)\ :\Gamma_{\rm ini}(t-t'):\ V(T_t)^T. \tag{26}$$

To obtain the state within the selected temporal mode, we integrate the quadrature variables over the relevant filter functions, $f_A(t), f_B(t)$, for example,

$$\hat{x}_A = \int_{-\infty}^{\infty} f_A(t)\hat{x}_{\rm A,bs}(t)dt. \tag{27}$$

When calculating the elements of the covariance matrix Γ, we can move the integration outside the expectation values, e.g.

$$\begin{aligned} :\Gamma_{13}: &= 2\langle :\Delta\hat{x}_A\Delta\hat{x}_B:\rangle \\ &= 2\langle :\int f_A(t)\Delta\hat{x}_{\rm A,bs}(t)dt \int f_B(t')\Delta\hat{x}_{\rm B,bs}(t')dt':\rangle \\ &= \int f_A(t)f_B(t')\ 2\langle :\Delta\hat{x}_{\rm A,bs}(t)\Delta\hat{x}_{\rm B,bs}(t'):\rangle dtdt' \\ &= \int f_A(t)f_B(t')\ :\Gamma_{\rm bs,13}(t-t'):\ dtdt'. \end{aligned} \tag{28}$$

Losses in both modes, as well as the trigger frequency filtering can be incorporated in the filter functions (see later). Therefore, the final matrix is

$$:\Gamma: = \iint \mathbf{f}(t)^T\ :\Gamma_{\rm bs}(t-t'):\ \mathbf{f}(t')\ dtdt', \tag{29}$$

with $\mathbf{f}(t) = {\rm diag}(f_A(t), f_A(t), f_B(t), f_B(t))$, and, remembering to put back the vacuum:

$$\Gamma = :\Gamma: +\Gamma_{\rm vac}. \tag{30}$$

3.3.2. Displacement vector

With a displacement $\hat{D}_B(\beta) = \hat{D}_B\big(|\beta|e^{i\phi_{\rm disp}}\big)$ in mode B, the displacement vector is

$$\mathbf{d} = \sqrt{2}|\beta|\ (0, 0, \cos\phi_{\rm disp}, \sin\phi_{\rm disp})^T. \tag{31}$$

The photon number in the mode due to this displacement is of course $n_{\rm disp} = |\beta|^2$. On the other hand, from $n = (\langle :\Delta\hat{x}^2: \rangle + \langle :\Delta\hat{p}^2: \rangle)/2$, the photon number due to the squeezing can be obtained as

$$n_{\rm sq} = \frac{1}{4}\left(:\Gamma_{33}: + :\Gamma_{44}:\right). \tag{32}$$

The photon numbers are not directly experimentally accessible, but they are proportional to the detected APD click rates, so we can get $|\beta|$ and the displacement vector in terms of these rates:

$$|\beta| = \sqrt{\frac{n_{\rm disp}}{n_{\rm sq}} n_{\rm sq}} = \sqrt{\frac{R_{\rm disp}}{R_{\rm sq}} \frac{:\Gamma_{33}: + :\Gamma_{44}:}{4}}\ , \tag{33}$$

$$\mathbf{d} = \sqrt{\frac{R_{\rm disp}}{R_{\rm sq}} \frac{:\Gamma_{33}: + :\Gamma_{44}:}{2}}\ (0, 0, \cos\phi_{\rm disp}, \sin\phi_{\rm disp})^T\ . \tag{34}$$

3.3.3. Mode functions

In the approach taken here, the filter functions play two different roles:

(1) To model the physical effect on the correlation matrix by losses and trigger filtering.
(2) To describe the actual observed temporal mode.

#2 is the original meaning of the mode function, but #1 can be included very nicely.

For the signal (mode A), the observed mode is the temporal filter applied to the raw homodyne data in post-processing. This can be chosen freely, but we always use the experimentally most reasonable function which is

$$\psi_A(t) = \sqrt{\mathcal{N}_A}\left(\frac{e^{-\gamma|t|}}{\gamma} - \frac{e^{-\kappa|t|}}{\kappa}\right), \tag{35}$$

with normalization $\mathcal{N}_A = \gamma^3\kappa^3(\gamma+\kappa)/(\gamma^4 + \gamma^3\kappa - 4\gamma^2\kappa^2 + \gamma\kappa^3 + \kappa^4)$. This is the double-sided exponential from the OPO output correlations, smoothened by the frequency filtering of the trigger. Including the overall signal efficiency gives the filter function

$$f_A(t) = \sqrt{\eta_A}\psi_A(t). \tag{36}$$

The APD detection time is very short relative to the correlation time, so the temporal mode can be taken to be a delta function:

$$\psi_B(t) = \delta(t). \tag{37}$$

The frequency filtering, however, has the effect that the photons arriving at the APD has been delayed relative to their correlated twins in the signal path. This can be taken into account by convoluting the mode function with the filter response, which gives (assuming the single

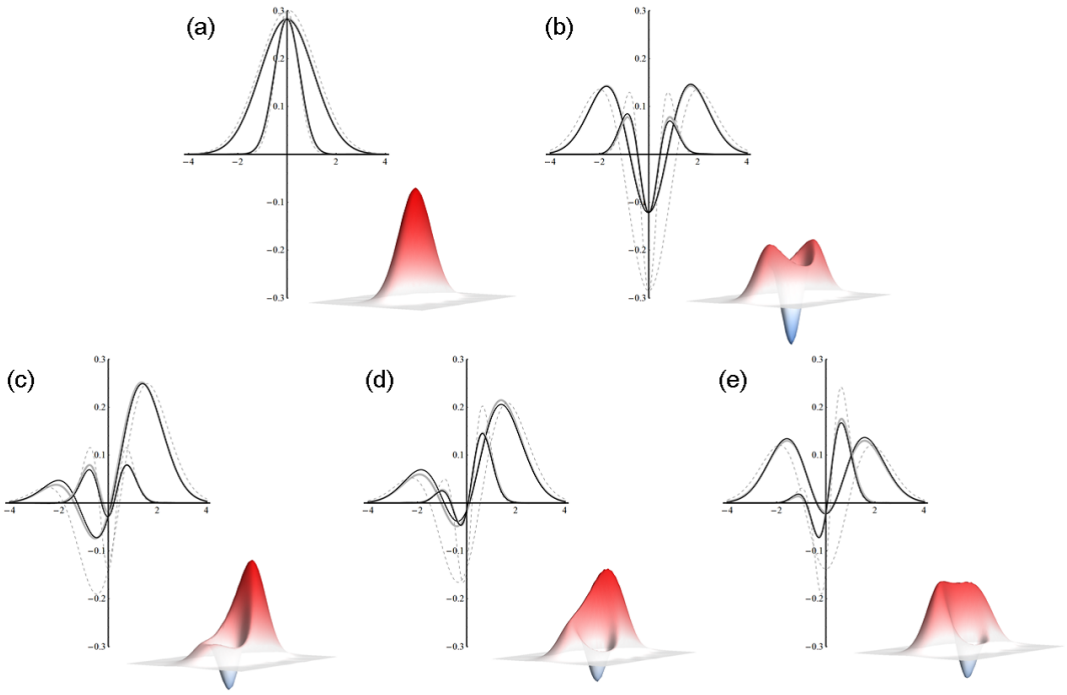

Figure 2. Wigner functions of the squeezed qubit states (a) $\theta = 0°$, (b) $\theta = 180°$, and (c), (d), (e), $\theta = 100°$ with $\varphi = 0°$, $45°$, $90°$. The narrow curves are $W(0,p)$ while the broader ones are $W(x,0)$. Numerical results from the multimode model (thick gray line) and the experimental results (*22*) (thinner black line) show good agreements. Parameters for model calculation are listed in Table 1. Dashed lines are the lossless model ($T_t \to 1$, $\eta_A = \eta_B = \chi = 1$, $\kappa \to \infty$, $R_{\rm dc} = 0$). Note that $T_t \to 1$ excludes the vacuum noise invasion from the unused input port of the beam splitter as well as the possibility of detecting multiple photons at the APD. Three dimensional figures are the experimental Wigner functions.

Lorentzian filter)

$$f_B(t) = \sqrt{2\kappa\eta_B}e^{\kappa t} \ , \quad \text{for } t \le 0 \text{ and 0 otherwise.} \tag{38}$$

The overall trigger efficiency was also included in the filter function.

Both filter functions assume a photon click at time $t = 0$. Due to the inclusion of losses, they are not normalized to 1.

4. Numerical results and comparison with experiments

In Fig. 2, the Wigner functions of the squeezed qubit states computed from Eq. (14) are plotted with the experimentally reconstructed Wigner functions in (*22*). The model simulates experimental outcomes well. Note that the model does not include any free parameters, i.e. the parameters in Table 1 are based on the experimental estimations. In the same figure, we also plot theoretical Wigner functions for the output states generated from a lossless cw setup, where "lossless" means all imperfections and effects of trigger filtering are excluded in the calculation (see the caption). Higher discrepancies between the Wigner functions with and without imperfections are observed at the negative part of the Wigner functions. The negativity of Wigner function, a quasi-probability distribution, reflects the strong non-classicality of the state and the discrepancies show how fragile the non-classicality is.

It should be noted that an output state from the lossless cw setup still includes some intrinsic imperfections due to the multimode nature of the cw beam. The difference between a squeezed qubit and that generated from the multimode model is estimated by taking their fidelity. Fidelity

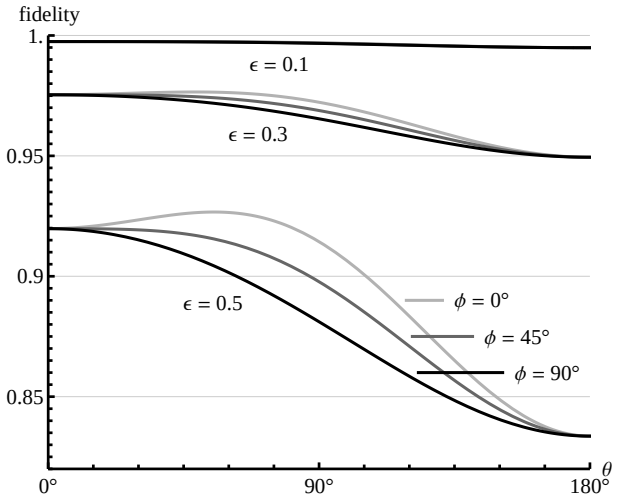

Figure 3. Fidelities between ideal squeezed qubits and the states generated from the lossless cw model are plotted for three different phases ($\varphi = 0°, 45°, 90°$) . For each pump level, $\epsilon = 0.1$, 0.3, and 0.5, the squeezing parameters for ideal squeezed qubits are chosen as $r = 0.15$, 0.45, and 0.77, these maximize the fidelity for essentially all θ.

between the photon subtracted state from a cw source (22) and an ideal squeezed qubit (3) are calculated as

$$F = \langle \mathrm{SQ}(\theta,\varphi)|\hat{\rho}_{\mathrm{out}}|\mathrm{SQ}(\theta,\varphi)\rangle = 2\pi \iint_{-\infty}^{\infty} W_{\mathrm{SQ}}(x,p) W_{\mathrm{out}}(x,p)\, dxdp, \tag{39}$$

where $\hat{\rho}_{\mathrm{out}}$ is the density matrix of the conditional output state $W_{\mathrm{out}}(x,p)$ and $W_{\mathrm{SQ}}(x,p)$ is the Wigner function of the ideal squeezed qubit (see Appendix). Figure 3 shows the fidelity between ideal squeezed qubits and the squeezed qubits calculated from the lossless cw model for different squeezing levels. The cw scheme works better for smaller θ, that is for qubits including a squeezed vacuum with higher ratio. This is also reflected in the fragility of the negativity of the Wigner function as seen in squeezed single photons. For reference, the experimentally obtained fidelities in (*22*) were in the range of 0.66–0.96.

In general, the fidelity decrease is caused by 1) the decoherence inside the qubit space, and 2) dissipation of the population to the outside of the qubit space. The signal space for the squeezed qubit is in principle spanned by a two-dimensional squeezed photon number basis $\{\hat{S}(r)|0\rangle, \hat{S}(r)|1\rangle\}$. We plot the density matrices of the squeezed qubit states from the lossless cw model and the experimental results in Figs. 4 and 5, respectively, in the bases of photon number state and squeezed photon number state. The former basis represents the continuous variable nature of the states while the latter basis shows how the states deviate from a squeezed qubit.

The figures show that the output states from the lossless cw model are well distributed in the 2×2 squeezed qubit space while non-negligible fractions in the squeezed two-photon state appear in the experimental output states. The fidelity decrease due to the cw nature of the setup therefore mainly originates from decoherence inside the qubit space. This is understood as follows. The cw squeezed beam is intuitively a sequence of light packets with extents given by Eqs. (5) and (6). Due to the finite overlap between these packets there is a finite probability that the subtracted photon comes from outside the packet of interest. This results in the conditional output of a statistical mixture between a coherently photon subtracted state and a squeezed vacuum, i.e. a decohered state inside the qubit space. On the other hand, practical imperfections, such as losses, more easily spread the conditional output state beyond the qubit space.

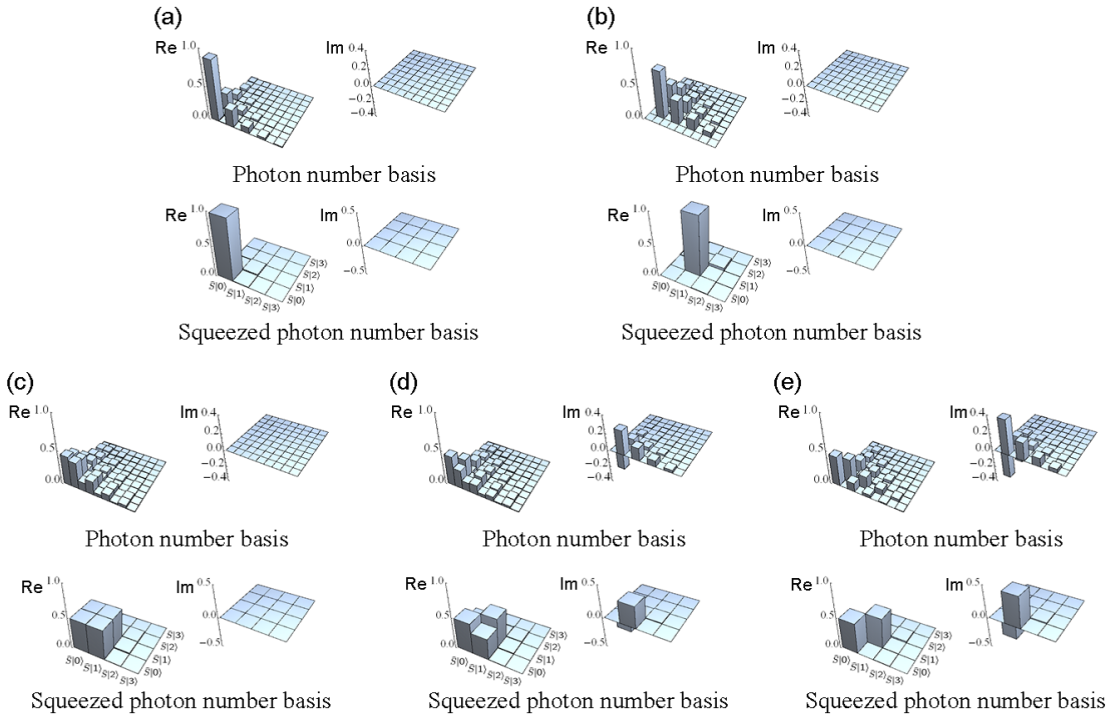

Figure 4. Density matrices of the squeezed qubits generated from the lossless cw model in photon number state and squeezed photon number state bases with (a) $\theta = 0°$, (b) $\theta = 180°$, and (c), (d), (e), $\theta = 90°$ with $\varphi = 0°$, $45°$, $90°$. The pump level is $\epsilon = 0.3$ and the squeezing parameter for the squeezed photon number basis is $r = 0.45$.

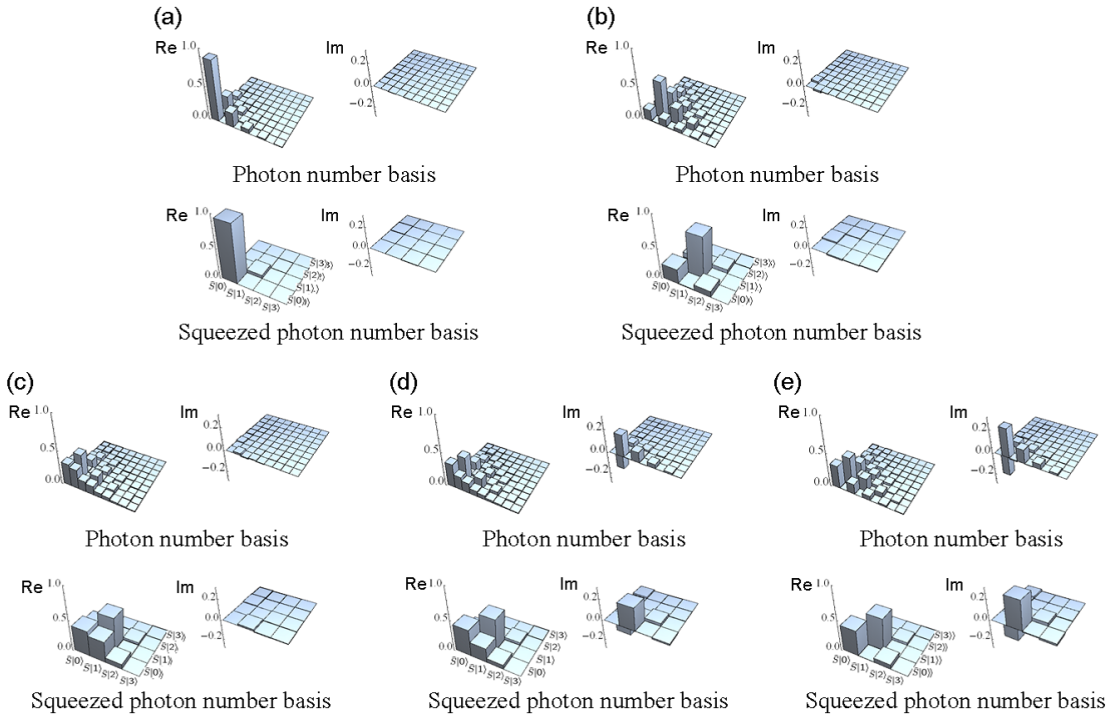

Figure 5. Density matrices of the squeezed qubits observed in (*22*) in photon number state and squeezed photon number state bases with (a) $\theta = 0°$, (b) $\theta = 180°$, and (c), (d), (e), $\theta = 90°$ with $\varphi = 0°$, $45°$, $90°$. The pump level is $\epsilon = 0.3$ and the squeezing parameter for the squeezed photon number basis is $r = 0.45$.

5. Conclusions

In this paper, we have described a fully multimode model of the arbitrary squeezed qubit generation in a continuous variable system. The model agrees well with our experimental results without taking free fitting parameters. We have also discussed the lossless cw model, in which any practical imperfections are excluded, and clarified the fundamental limit of the cw setting. We have shown that the fidelity to the ideal squeezed qubit can be higher than 95% for moderate or small squeezing. Moreover, the discrepancy of the fidelity is due to the decoherence inside the squeezed qubit space, which could be more easily corrected than the energy dissipation in future QIP architectures, such as quantum error correction. In addition, it is also worth to note that the cw source with multiple photon subtraction has an intrinsic multimode structure and is useful for generating larger cat-like states (*5, 26, 27*). Finally, if the input state instead of squeezed vacuum were one of the cat-like states $|\alpha\rangle \pm |-\alpha\rangle$, our scheme presented here can generate arbitrary qubits in a coherent state basis. This is possible by combining our technique with the already existing cat-like states (*1–6*), which will provide a basic resource for CSQC and its applications, such as quantum collective decoding.

6. Acknowledgement

MT has been supported by MEXT Grant-in-Aid for Young Scientists (B) 22740270.

Appendix A. Wigner function of an ideal squeezed qubit

In this appendix, we draw the Wigner function of the ideal squeezed qubit, $W_{\rm SQ}(x,p) = (2\pi)^{-1}\int e^{iyp}\langle x-y/2\,|{\rm SQ}\rangle\,\langle {\rm SQ}|\,x+y/2\rangle dy$ for the completeness of the paper. To calculate it, we need the wave functions of the squeezed vacuum and the squeezed photon:

$$\langle x|\,\hat{S}(r)\,|0\rangle = (\pi e^{2r})^{-1/4}e^{-x^2/2e^{2r}}, \tag{A1}$$

$$\begin{aligned}\langle x|\,\hat{S}(r)\,|1\rangle &= \langle x|\,\frac{1}{\sinh r}\hat{a}\hat{S}(r)\,|0\rangle \\ &= \frac{1}{\sqrt{2}\sinh r}\left(x+\frac{d}{dx}\right)\langle x|\,\hat{S}(r)\,|0\rangle \\ &= \sqrt{\frac{2}{\sqrt{\pi}e^{3r}}}\,xe^{-x^2/2e^{2r}}.\end{aligned} \tag{A2}$$

This gives the following expression for the squeezed qubit Wigner function:

$$W_{\rm SQ}(x,p) = \frac{1}{\pi}e^{-e^{-2r}x^2-e^{2r}p^2}\left(\cos\theta+(1-\cos\theta)\Big(\frac{x^2}{e^{2r}}+\frac{p^2}{e^{-2r}}\Big)+\sqrt{2}\Big(\cos\phi\frac{x}{e^r}+\sin\phi\frac{p}{e^{-r}}\Big)\sin\theta\right). \tag{A3}$$

References

(1) A. Ourjoumtsev, R. Tualle-Brouri, J. Laurat, and P. Grangier, *Science* **312**, 83 (2006).
(2) J. S. Neergaard-Nielsen, B. M. Nielsen, C. Hettich, and K. Mølmer, and E. S. Polzik, *Phys. Rev. Lett.* **97**, 083604 (2006).
(3) K. Wakui, H. Takahashi, A. Furusawa, and M. Sasaki, *Opt. Express* **15**, 3568 (2007).
(4) A. Ourjoumtsev, H. Jeong, R. Tualle-Brouri, and P. Grangier, *Nature* **448**, 784 (2007).
(5) H. Takahashi, K. Wakui, S. Suzuki, M. Takeoka, K. Hayasaka, A. Furusawa, and M. Sasaki *Phys. Rev. Lett.* **101**, 233605 (2008).

(6) T. Gerrits, S. Glancy, T. S. Clement, B. Calkins, A. E. Lita, A. J. Miller, A. L. Migdall, S. W. Nam, R. P. Mirin, and E. Knill, arXiv:1004.2727 [quant-ph].
(7) E. Bimbard, N. Jain, A. MacRae, and A. I. Lvovsky, *Nature Photonics* **4**, 243 (2010).
(8) A. Ourjoumtsev, A. Dantan, R. Tualle-Brouri, and P. Grangier, *Phys. Rev. Lett.* **98**, 030502 (2007).
(9) H. Takahashi, J. S. Neergaard-Nielsen, M. Takeuchi, M. Takeoka, K. Hayasaka, A. Furusawa, and M. Sasaki *Nature Photonics* **4**, 178 (2010).
(10) A. Zavatta, V. Parigi, M. S. Kim, H. Jeong, and M. Bellini, *Phys. Rev. Lett.* **103**, 140406 (2009).
(11) P. T. Cochrane, G. J. Milburn, and W. J. Munro, *Phys. Rev. A* **59**, 2631 (1999).
(12) H. Jeong and M. S. Kim, *Phys. Rev. A* **65**, 042325 (2002).
(13) T. C. Ralph, A. Gilchrist, G. J. Milburn, W. J. Munro, and S. Glancy, *Phys. Rev. A* **68**, 042319 (2003).
(14) H. Jeong and T. C. Ralph, in *Quantum Information with Continuous Variables of Atoms and Light*, edited by N. Cerf, G. Leuchs, and E. Polzik; Imperial College Press: London, 2007, Chapter 9.
(15) A. P. Lund, T. C. Ralph, and H. L. Haselgrove, *Phys. Rev. Lett.* **100**, 030503 (2008).
(16) A. S. Holevo, *IEEE Trans. Inf. Theory* **44**, 269 (1998); B. Schumacher and M. D. Westmoreland, *Phys. Rev. A* **56**, 131 (1997). See also M. A. Nielsen and I. L. Chuang, *Quantum Computation and Quantum Information*; Cambridge University Press: Cambridge, 2000, Chapter 12.
(17) V. Giovannetti, S. Guha, S. Lloyd, L. Maccone, J. H. Shapiro, and H. P. Yuen, *Phys. Rev. Lett.* **92**, 027902 (2004).
(18) M. Sasaki, T. Sasaki-Usuda, M. Izutsu, and O. Hirota, *Phys. Rev. A* **58**, 159 (1998).
(19) M. Fujiwara, M. Takeoka, J. Mizuno, and M. Sasaki, *Phys. Rev. Lett.* **90**, 167906 (2003).
(20) M. Takeoka, M. Fujiwara, J. Mizuno, and M. Sasaki, *Phys. Rev. A* **69**, 052329 (2004).
(21) M. Takeoka and M. Sasaki, *Phys. Rev. A* **75**, 064302 (2007).
(22) J. S. Neergaard-Nielsen, M. Takeuchi, K. Wakui, H. Takahashi, K. Hayasaka, M. Takeoka, and M. Sasaki, *Phys. Rev. Lett.* **105**, 053602 (2010).
(23) C. W. Gardiner, P. Zoller, *Quantum Noise*, Springer-Verlag, Berlin (2000).
(24) The trigger filtering consists of two Fabry-Perot cavities, each with a Lorentzian transmission spectrum. However, one cavity is considerably narrower than the other, so we model the total effect of the filtering as a single Lorentzian filter with a bandwidth slightly lower than that of the narrowest cavity.
(25) K. Mølmer, *Phys. Rev. A* **73**, 063804 (2006).
(26) M. Takeoka, H. Takahashi, and M. Sasaki, *Phys. Rev. A* **77**, 062315 (2008).
(27) M. Sasaki, M. Takeoka, and H. Takahashi, *Phys. Rev. A* **77**, 063840 (2008).